The Scaling of Blood Flow Resistance: From a Single Vessel to the Entire Distal Tree

Yunlong Huo and Ghassan S. Kassab*
Department of Biomedical Engineering, Surgery, and Cellular and Integrative Physiology, Indiana University-Purdue University Indianapolis, Indianapolis, Indiana

ABSTRACT Although the flow resistance of a single vessel segment is easy to compute, the equivalent resistance of a network of vessel segments or the entire vasculature of an organ is difficult to determine in an analytic form. Here, we propose what we believe is a novel resistance scaling law for a vascular tree (i.e., the resistance of a vessel segment scales with the equivalent resistance of the corresponding distal tree). The formulation can be written as $(R_s/R_c) \propto (L_s/L_c)$ (where R_s and L_s are the resistance and length of a vessel segment, respectively, and R_c and L_c are the equivalent resistance and total length of the corresponding distal tree, respectively), which was validated for the coronary vascular systems of the heart. The scaling law was also shown to apply to the vascular systems of the lung, mesentery, muscle, eye, and so on. The novel resistance scaling law, coupled with the 3/4-power scaling law for metabolic rates, can predict several structure-function relations of vascular trees, albeit with a different exponent. In particular, the self-similar nature of the scaling law may serve as a diagnostic tool with the help of noninvasive imaging modalities.

INTRODUCTION

The biological transport structure has significant similarities across species despite remarkable diversity and size. The vascular tree, whose function is to transport fluid within an organism, is a major distribution system that has fractal and scaling characteristics (1–4). A fundamental functional parameter of a vessel segment or a tree is the hydraulic resistance to flow, which determines the transport efficiency (5).

In a hydrodynamic analysis of mammalian and plant vascular networks, a mathematical model of 3/4-power scaling for metabolic rates has been reported (6). A number of scaling relations of structure-function features were further proposed for body size (7,8), temperature (9), species abundance (8), body growth (9,10), and so on. Although the 3/4-scaling law was originally derived through a hemodynamic analysis in the vascular tree system, one basic structure-function scaling feature of vascular trees remains unclear: ''How does the resistance of a vessel branch scale with the equivalent resistance of the corresponding distal tree''?

In this study, we propose what we believe is a novel scaling law of a single vessel resistance to the corresponding distal tree. The scaling law is validated in both the actual asymmetric coronary trees and the idealized symmetric vascular trees for which there exist morphometric data in the literature. The scaling law, also coupled with the 3/4-power scaling law ($Q_s \propto M^{3/4}$, where Q_s is the inlet flow rate of a tree and M is the perfused mass by the tree), can predict several structure-function scaling laws of vascular trees (11–13). The significance of the novel resistance scaling law is elaborated physiologically and, potentially, clinically.

THEORY

Several concepts are first defined to formulate the resistance scaling law. A vessel segment is defined as a stem, and the tree distal to the stem is defined as a crown (see Fig. 1 in Kassab (11)). Obviously, an entire tree consists of many stem-crown units down to the smallest arterioles or venules. The capillary network (vessel diameter <8 μm) (14) is excluded from this analysis because it is not treelike in structure. A stem is assumed to be a cylindrical tube with no consideration of vessel tapering and other nonlinear effects because they play a relatively minor role in determining the hemodynamics of the entire tree (6). Through the well-known Hagen-Poiseuille law, the resistance of the steady laminar flow in a stem of an entire tree, $R_s = \frac{\Delta P_s}{Q_s}$ (where ΔP_s is the pressure gradient along the stem and Q_s is the volumetric flow rate through the stem), can be written as

$$R_s = \frac{128\mu L_s}{\pi D_s^4} = K_s \frac{L_s}{D_s^4}, \tag{1}$$

where D_s and L_s are the diameter and length of the stem, respectively. The fluid viscosity, μ, and $K_s = 128\mu/\pi$ are considered constant for the stem. Furthermore, the resistance of a crown, $R_c = \frac{\Delta P_c}{Q_s}$ (where ΔP_c is the pressure gradient in the crown from the stem to the terminal vessels), is proposed as follows (see the Appendix for derivations):

$$R_c = K_c \frac{L_c}{D_s^4}, \tag{2a}$$

Submitted July 24, 2008, and accepted for publication September 22, 2008.

*Correspondence: gkassab@iupui.edu

Editor: Elliot L. Elson.

0006-3495/09/01/0339/8 $2.00

doi: 10.1016/j.bpj.2008.09.038

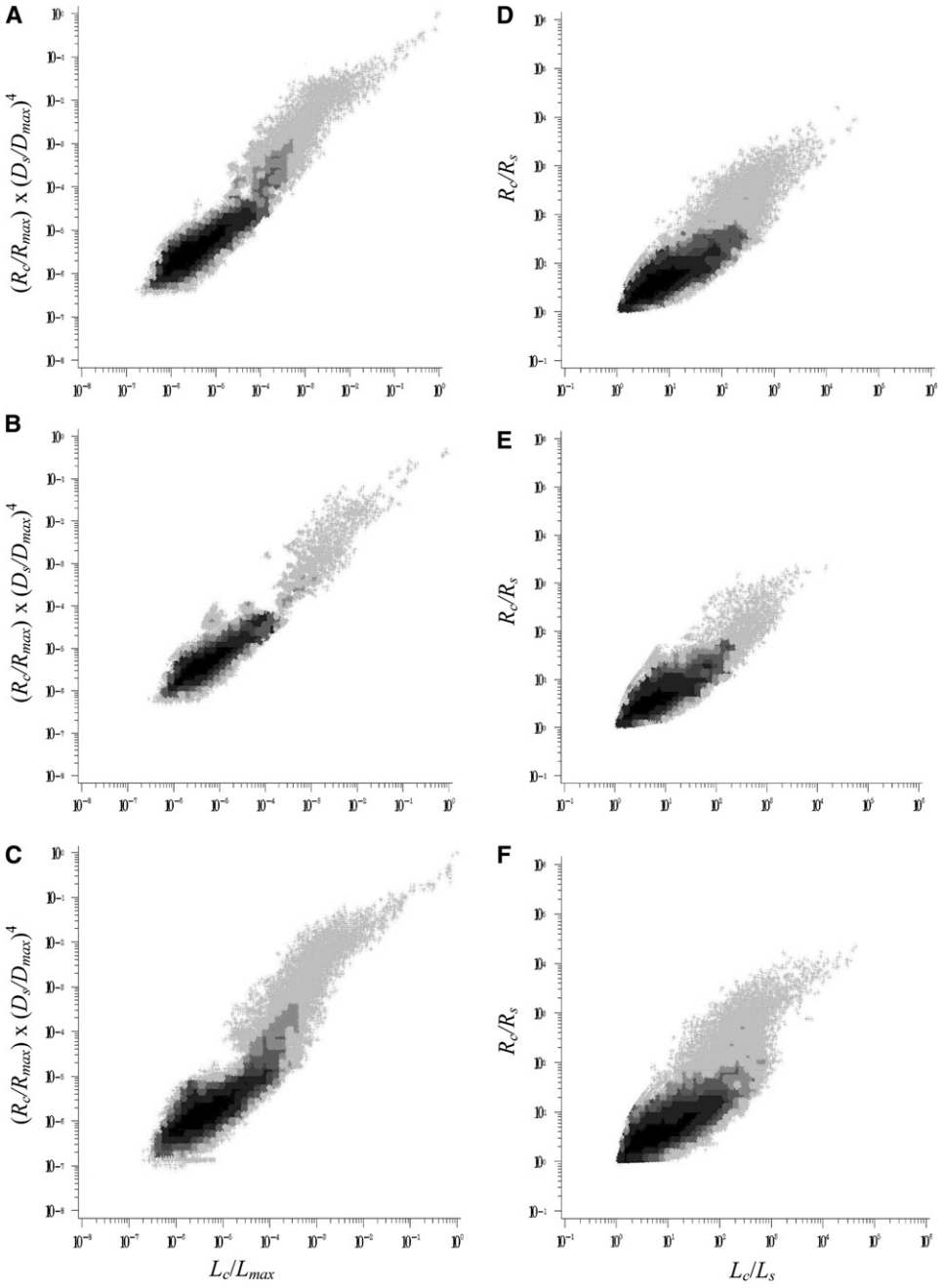

FIGURE 1 Relationship between $(R_c/R_{max}) \times (D_s/D_{max})^4$ and normalized crown length (L_c/L_{max}) in the asymmetric entire (*A*) LAD, (*B*) LCx, and (*C*) RCA trees of pig, which include 946,937, 571,383, and 836,712 stem-crown units, respectively. (*D–F*) Relationship between R_c/R_s and L_c/L_s in the LAD, LCx, and RCA trees of pig corresponding to (*A–C*).

where L_c is the crown length that is defined as the sum of the lengths of each vessel in the crown and D_s is the diameter of the stem vessel proximal to the crown. K_c is a constant that depends on the branching ratio, diameter ratio, total number of tree generations, and viscosity in the crown. Since Eq. 2a is applicable to any stem-crown unit, we obtain $R_{max} = K_c L_{max}/D_{max}^4$ such that $K_c = R_{max} \times D_{max}^4/L_{max}$, where D_{max}, L_{max}, and R_{max} correspond, respectively, to the most proximal stem diameter, the cumulative vascular length, and the total resistance of the entire tree. In the nondimensional form, Eq. 2a can be written as

$$\left(\frac{R_c}{R_{max}}\right) \times \left(\frac{D_s}{D_{max}}\right)^4 = A_1\left(\frac{L_c}{L_{max}}\right). \quad (2b)$$

Parameter A_1 in Eq. 2b should be equal to one. From Eqs. 1 and 2a, we obtain the desired resistance scaling relation between a single vessel (a stem) and the distal crown tree:

$$\left(\frac{R_s}{R_c}\right) = \frac{K_s}{K_c}\left(\frac{L_s}{L_c}\right). \quad (3)$$

Equations 1–3 relate the resistance of a single vessel to the corresponding distal tree.

METHODS

Morphometric vascular trees

The realistic asymmetric coronary arterial trees of hearts and idealized symmetric vascular trees of many organs were used to verify the proposed resistance scaling law. First, the asymmetric coronary arterial tree has been reconstructed in pig hearts by using the growth algorithm introduced by Mittal et al. (15) based on the measured morphometric data of Kassab et al. (16). Briefly, vessels ≥ 40 μm were reconstructed from cast data, whereas vessels <40 μm were reconstructed from histological data. After the tree was reconstructed, each vessel was identified by a diameter-defined Strahler order (16), which was developed based on the Strahler system (17).

Furthermore, symmetric vascular trees of many organs were constructed in the Strahler system, based on available literature (18–29). The pulmonary arterial tree of rats was obtained from the study of Jiang et al. (18); the pulmonary arterial/venous trees of cats from Yen et al. (19,20); the pulmonary arterial trees of humans from Singhal et al. (21,22) and Huang et al. (23); the pulmonary venous trees of humans from Horsfield and Gordon (24) and Huang et al. (23); the skin muscle arterial tree of hamsters from Bertuglia et al. (25); the retractor muscle arterial tree of hamsters from Ellsworth et al. (26); the mesentery arterial tree of rats from Ley et al. (27); the sartorius muscle arterial tree of cats from Koller et al. (28); and the bulbular conjunctiva arterial/venous trees of humans and the omentum arterial tree of rabbits from Fenton and Zweifach (29).

Data analysis

For the asymmetric coronary arterial trees, full tree data are presented as log-log density plots showing the frequency of data because of the enormity of data points, i.e., the darkest shade reflects the highest frequency or density and the lightest shade reflects the lowest frequency (30). The nonlinear regression (SigmaStat 3.5, Systat Software, San Jose, CA) was used to analyze the data in both the asymmetric and symmetric trees, which uses the Marquardt-Levenberg algorithm (nonlinear regression) to find the coefficients (parameters) of the independent variables that give the "best fit" between the equation and the data.

RESULTS

Validation of the resistance scaling law in entire vascular trees

We validated the predictions of these novel scaling laws in both the asymmetric coronary trees and the symmetric vascular trees for which there exist morphometric data in the literature (e.g., vessels of various skeletal muscles, mesentery, omentum, and conjunctiva) (18–29).

First, we analyzed the entire asymmetric coronary LAD (left anterior descending artery), LCx (left circumflex artery), and RCA (right coronary artery) trees with several millions of vessels (15,16). Fig. 1, *A–C*, shows a log-log plot of $(R_c/R_{max}) \times (D_s/D_{max})^4$ as a function of normalized crown length (L_c/L_{max}) for LAD, LCx, and RCA trees, respectively. Through the Marquardt-Levenberg algorithm with the exponents of L_c/L_{max} constrained to one, parameter A_1 in Eq. 2b has a value of 1.027 ($R^2 = 0.990$), 0.993 ($R^2 = 0.997$), and 1.084 ($R^2 = 0.975$) for LAD, LCx, and RCA trees, respectively. The values of A_1 obtained from morphometric data are in agreement with the theoretical value of one. Corresponding to Fig. 1, *A–C*, Fig. 1, *D–F*, shows a log-log plot of R_c/R_s as a function of L_c/L_s. Parameter K_s/K_c in Eq. 3 has a value of 2.647 ($R^2 = 0.954$), 2.943 ($R^2 = 0.918$), and 2.147 ($R^2 = 0.909$) for LAD, LCx, and RCA trees, respectively.

Furthermore, Fig. 2, *A* and *B*, shows the log-log plots of $(R_c/R_{max}) \times (D_0/D_{max})^4$ and R_c/R_s as a function of L_c/L_{max} and L_c/L_s, respectively, in the vascular trees of various species (16,18–29). Corresponding to Fig. 2, *A* and *B*, we used the Marquardt-Levenberg algorithm to calculate the parameters A_1 and K_s/K_c in Eqs. 2b and 3, respectively, whereas the exponents of L_c/L_{max} and L_c/L_s were constrained to one. Parameters A_1 in Eq. 2b and K_s/K_c in Eq. 3 with correlation coefficient for various species (16,18–29) are listed in Table 1. The standard errors and coefficients of variations are used as a measure of the variance or spread around the regression line. The standard

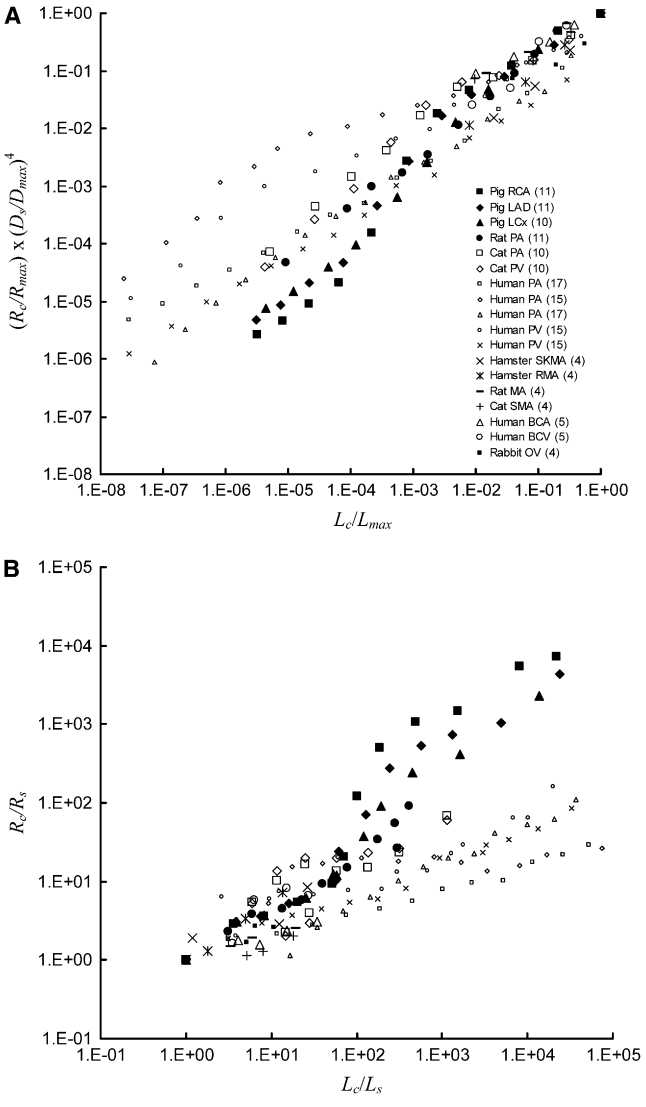

FIGURE 2 (*A*) Corresponding to Table 1, the relationship between $(R_c/R_{max}) \times (D_s/D_{max})^4$ and normalized crown length (L_c/L_{max}) in the symmetric vascular tree for various species (16,18–29). (*B*) Corresponding to *A*, the relationship between R_c/R_s and L_c/L_s.

TABLE 1 Parameters A_1 in Eq. 2b and $(K_s/K_c)_{ML}$ in Eq. 3 with correlation coefficient calculated from the Marquardt-Levenberg algorithm, respectively, for various species (16,18–29)

Species	Vessel (N)	A_1	R^2	$(K_s/K_c)_{ML}$	R^2	Reference
Pig	RCA (11)	1.06	0.93	2.38	0.88	16
Pig	LAD (11)	1.02	0.99	5.32	0.97	16
Pig	LCx (10)	1.01	0.98	5.79	0.99	16
Rat	PA (11)	1.07	0.90	5.03	0.86	18
Cat	PA (10)	1.03	0.98	24.3	0.90	19
Cat	PV (10)	1.02	0.99	14.1	0.85	20
Human	PA (17)	0.97	0.98	2002.0	0.85	21
Human	PA (15)	0.98	0.98	1956.0	0.91	23
Human	PA (17)	0.95	0.97	445.0	0.80	22
Human	PV (15)	0.97	0.98	726.0	0.96	21
Human	PV (15)	0.94	0.95	96.3	0.95	24
Hamster	SKMA (4)	0.97	0.98	1.16	0.92	25
Hamster	RMA (4)	1.00	1.00	1.76	0.98	26
Rat	MA (4)	1.11	0.83	4.99	0.55	27
Cat	SMA (4)	1.04	0.96	6.66	0.61	28
Human	BCA (5)	1.11	0.88	7.40	0.60	29
Human	BCV (5)	1.10	0.86	2.35	0.54	29
Rabbit	OV (4)	0.88	0.90	3.11	0.68	29

N, total number of Strahler orders in the respective vascular tree; RCA, right coronary artery; LAD, left anterior descending artery; LCx, left circumflex artery; PA, pulmonary artery; PV, pulmonary vein; SKMA, skin muscle arteries; SMA, sartorius muscle arteries; MA, mesentery arteries; OV, omentum veins; BCA, bulbular conjunctiva arteries; RMA, retractor muscle artery; BCV, bulbular conjunctiva vein.

errors and parameter coefficients of variation of A_1 in Table 1 are $<0.1\%$ and $<10.0\%$, respectively. The data in Table 1 have a mean value (averaged over all organs and species) of 1.01 ± 0.06 for parameter A_1. Using the same Marquardt-Levenberg algorithm, a nonlinear regression fit of all raw data yields a mean of 1.01 ($R^2 = 0.95$) for parameter A_1. Both the mean value and the nonlinear regression fit of all data agree with the theoretical value of one. Fig. 2 *B* shows much smaller R_c/R_s in the pulmonary vascular tree than other organs at the same value of L_c/L_s. Accordingly, the K_s/K_c values (Table 1) are similar except for the pulmonary vasculature with a larger value. The K_s/K_c values are also calculated based on equations $K_s = 128\mu/\pi$ and $K_c = R_{max} \times D_{max}^4/L_{max}$, which is compared with the K_s/K_c values obtained from the Marquardt-Levenberg algorithm, as shown in Fig. 3. The viscosity is determined based on an empirical in vivo relation that depends on the vessel diameter (31). The comparison shows good agreement. The K_s/K_c values in the pulmonary vasculature have a larger value because the cross section area (CSA) of the pulmonary tree has a large increase from proximal to terminal vessels in the pulmonary tree and the resistance of the entire tree (R_{max}) is much smaller. The value of K_s/K_c in human pulmonary arterial and venous trees is even larger than that in cats and rats. From the definition of K_ε (see Appendix), it is noted that K_ε decreases with the increase of the total number of tree generations. The major reason for the large value of K_s/K_c is that the human pulmonary tree has many more

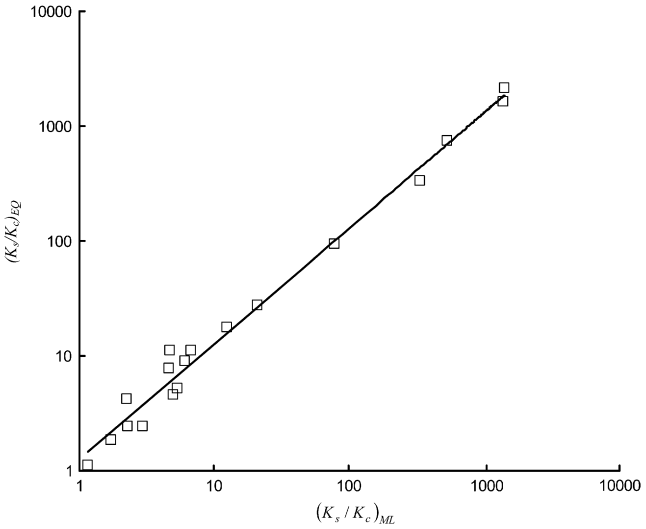

FIGURE 3 A comparison of $(K_s/K_c)_{ML}$ from the nonlinear regression of anatomical data and $(K_s/K_c)_{EQ}$ based on equations $K_s = 128\mu/\pi$ and $K_c = R_{max} \times D_{max}^4/L_{max}$. The comparison can be represented as $(K_s/K_c)_{EQ} = A \times (K_s/K_c)_{ML}^B$. When A is constrained to be 1 in the Marquardt-Levenberg algorithm, B has a value of 1 ($R^2 = 0.983$).

generations from the stem to each terminal, which is ~2 times larger than the pulmonary tree in cats and rats. Therefore the human pulmonary tree with more tree generations has a larger value of K_s/K_c. The agreement between experimental measurement and theoretical relations illustrates that the novel proposed resistance scaling law of Eqs. 2 and 3 can be applied to a general vascular tree down to the smallest arterioles or venules.

Resistance scaling law of partial vascular trees

Fig. 4, *A* and *B*, shows the relations between $(R_c/R_{max}) \times (D_s/D_{max})^4$ and normalized crown volume (L_c/L_{max}) and between R_c/R_s and L_c/L_s, respectively, in the LAD, LCx, and RCA epicardial trees. Parameter A_1 in Eq. 2b has a value of 0.902 ($R^2 = 0.907$), 0.895 ($R^2 = 0.887$), and 1.000 ($R^2 = 0.888$); and parameter K_s/K_c in Eq. 3 has a value of 3.29 ($R^2 = 0.875$), 3.48 ($R^2 = 0.816$), and 3.12 ($R^2 = 0.927$) for the LAD, LCx, and RCA epicardial trees, respectively.

DISCUSSION

This study provides what we believe is a novel resistance scaling law that relates the resistance of a vessel branch to the equivalent resistance of the corresponding distal tree in various vascular trees of different organs and species. The significance of the resistant scaling law is that the hydraulic resistance of a distal vascular tree can be estimated from the proximal vessel segment. This has wide implications, from understanding fundamental vascular design to the diagnosis of disease in the vascular system.

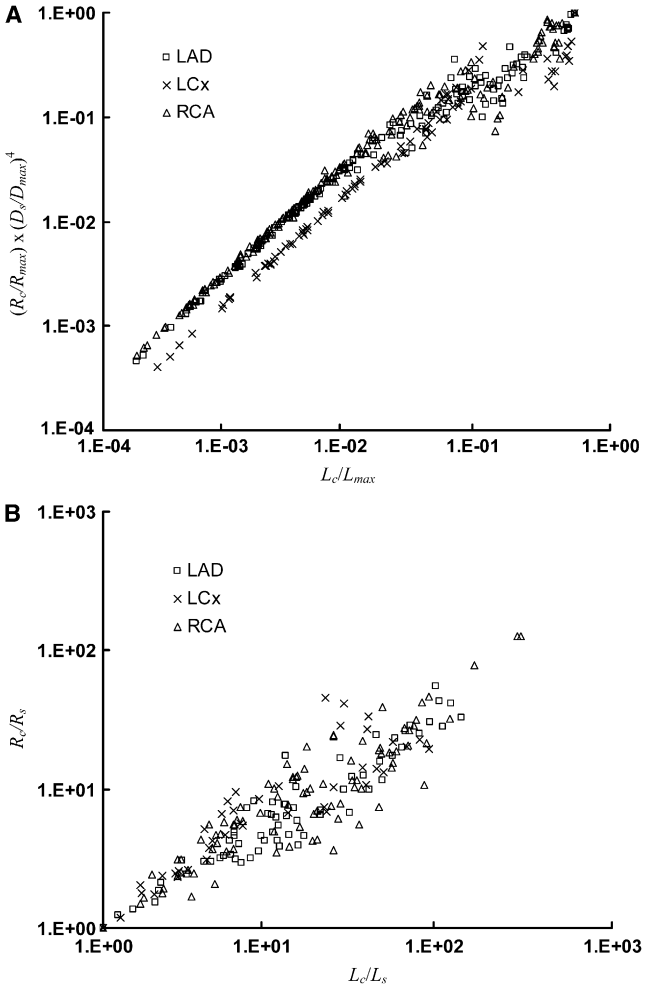

FIGURE 4 (*A*) Relationship between $(R_c/R_{max}) \times (D_s/D_{max})^4$ and normalized crown volume (L_c/L_{max}) in the LAD, LCx, and RCA epicardial trees of pig with diameter of mother vessels larger than 1 mm, which include 132, 90, and 192 vessel segments, respectively. (*B*) Relationship between R_c/R_s and L_c/L_s in the LAD, LCx, and RCA epicardial trees of pig corresponding to *A*.

The resistance scaling law

The mechanisms responsible for blood flow regulation in vascular trees are of central importance but are still poorly understood (32). The arteriolar beds are the major site of vascular resistance (33–36), which contributes to the maintenance and regulation of regional blood flow. Although arteriolar resistance plays an important role in the etiology of many diseases, in particular, hypertension (37–39), it has been difficult to predict the resistance in the arteriolar beds. The proposed resistance scaling law addresses this issue.

The resistance scaling laws (Eqs. 2 and 3) are derived based on the relation of diameter ratio $(\mathrm{DR} = D_i/D_{i-1})$, length ratio $(\mathrm{LR} = L_i/L_{i-1})$, and branching ratio $(\mathrm{BR} = N_i/N_{i-1})$ in a symmetric tree as $\mathrm{DR} = \mathrm{BR}^{-\frac{1}{2+\varepsilon}}$ and $\mathrm{LR} = \mathrm{BR}^{-\frac{1}{3}}$, where $\varepsilon = 0$ and $\varepsilon = 1$ represent the area preservation, $\pi D_{i-1}^2 = \mathrm{BR} \times \pi D_i^2$, and Murray's law, $\pi D_{i-1}^3 = \mathrm{BR} \times \pi D_i^3$, respectively. The parameter $K_c = K_s K_\varepsilon$ in Eq. 2 where K_ε depends on ε and the branching ratio and total number of generations, as shown in Appendix. The detailed formulations are outlined in the Appendix.

Although the total CSA may increase dramatically from the aorta to the arterioles, the variation is significantly smaller in most organs except for the lung. The increase of CSA toward the capillaries is typically inferred from the decrease in velocity. The velocity between the most proximal and distal levels in various organs of mammals is found to vary by about a factor of 5 (40–48) except for the pulmonary vascular trees (49,50). This is clearly reflected by Table 1, in which $K_s/K_c = \frac{1}{K_\varepsilon}$ is relatively small except for the pulmonary vasculature. This implies that wall shear stress increases from the arteries to the arterioles in most organs, which is consistent with previous measurements (30,43,44).

Structure-function scaling laws obtained from the resistance scaling law

A mathematical model (the 3/4-power scaling law) was derived in a symmetric vasculature to characterize the allometric scaling laws (6), based on the minimum energy theory. The 3/4-power scaling law can be written as $Q_s \propto M^{3/4}$, where Q_s is the volumetric flow rate of the aorta and M is body mass. In a stem-crown unit, Q_s is the volumetric flow rate of the stem and M is the mass perfused by the stem-crown unit. The volumetric flow rate of the stem is $Q_s = \pi D_s^2 U_s/4$, where D_s and U_s are, respectively, the diameter and the mean flow velocity of the stem (averaged over the cross section of stem). Similar to the model of West et al. (6), the pressure drop from the stem to the capillaries (ΔP_c) and the mean flow velocity of the stem (U_s) are independent of the perfused mass so that $D_s \propto M^{3/8}$ and the resistance of the crown $(R_c = \Delta P_c/Q_s)$ is inversely proportional to the volumetric flow rate $(R_c \propto Q_s^{-1} \propto M^{-3/4})$. Since $D_s \propto M^{3/8}$, $R_c \propto M^{-3/4}$, and K_c is a constant, Eq. 2 yields that the crown length $L_c \propto M^{3/4}$. The cumulative length-mass scaling in pig hearts, $L_c \propto M^{3/4}$, has recently been verified by our group (51). This relation, in conjunction with the flow-mass relation $(Q_s \propto M^{3/4})$, yields the flow-length relation $(Q_s \propto L_c)$ in the stem-crown unit, which has been previously validated (11).

Here, the crown length $L_c \propto M^{3/4}$ is different from the biological length $l \propto M^{1/4}$ (7). The biological length (l) is the cumulative length along a path from inlet (level zero) to the terminal (level N), whereas the crown length is the total length of all vessels from inlet to the terminals. Although the biological length shows that the vascular physiology and anatomy are four dimensional, the crown length depicts a 3/4-power relation between the total length of the entire/partial biological system and the perfused mass.

Clinical implications of the resistance scaling law

The self-similar nature of the structure-function scaling laws in Eqs. 2 and 3 implies that they can be applied to a partial tree clinically (e.g., a partial tree obtained from an

angiogram, computerized tomography, or magnetic resonance imaging). Here, we verified the hypothesis using the LAD, LCx, and RCA epicardial pig trees obtained from casts truncated at 1 mm diameter to mimic the resolution of noninvasive imaging techniques. The good agreement between experiments and theory, as shown in Fig. 4, illustrates that the resistance scaling laws can be applied to partial vascular trees as well as entire trees.

The resistance scaling law is fundamental to many diagnostic hemodynamic measurements (e.g., blood pressure, wedge pressure, total peripheral resistance, cardiac output, etc.). Specifically, the proportionality constant of the scaling law in the epicardial coronary arterial trees may serve as a diagnostic parameter of vascular function. The crown resistance for each primary branch can also be calculated from Eq. 2 or 3. The crown resistance in diseased heart with congestive heart failure or ischemia heart disease can be estimated based on flow rates obtained from noninvasive techniques (e.g., angiography, MRI, etc.) and pressure measurements. The deviations from established crown resistance of normal patients may emerge as diagnostic indices for various vascular diseases.

Critique of the resistance scaling law

The resistance scaling law was derived from a Taylor expansion that rigorously requires an infinite series. This implies that the scaling law should better predict those trees that have more generations. Furthermore, this study only considered the scaling relation in organs without substantial vascular tone. The balance between myogenic, flow-dependent, and metabolic flow control should be included in future studies.

Significance of the resistance scaling law

The novel resistance scaling law (Eq. 2) provides a theoretical and physical basis for understanding the hemodynamic resistance of the entire tree (or a subtree) and provides a rationale for clinical diagnosis. The scaling law illustrates the relationship between the structure (tree) and function (resistance) in which the crown resistance is proportional to the crown length and inversely proportional to the fourth power of stem diameter D_s^4. The small crown resistance corresponds to a small crown length, thus matching the transport efficiency of the crown. An increase of stem diameter can decrease the resistance, which may contribute to the self-scaling of a biological transport system (52–54). The novel scaling law provides an integration between a single vascular unit and the whole (millions of vessels) and imparts a rationale for the diagnosis of disease processes as well as the assessment of therapeutic trials.

APPENDIX

An idealized symmetric crown distal to the stem is composed of N_{total} levels or generations from the stem (level zero) to each terminal (the smallest arteriolar bifurcation, level N_{total}). The resistance of a symmetric crown, R_c, can be written as

$$R_c = R_s + \sum_{i=1}^{N_{\text{total}}} \frac{R_i}{N_i};\ R_i = \frac{128\mu L_i}{\pi D_i^4} = K_s \frac{L_i}{D_i^4};\quad i = 1, \cdots, N_{\text{total}}, \tag{A1}$$

where

$$R_s = \frac{128\mu L_s}{\pi D_s^4} = K_s \frac{L_s}{D_s^4} \text{ and } K_s = \frac{128\mu}{\pi},$$

and R_s, L_s, and D_s are the resistance, length, and diameter of the stem, respectively, and K_s is a constant. Similarly, R_i, L_i, and D_i are the resistance, length, and diameter of a vessel in level i, respectively, and N_i is the total number of vessels in level i. Here, the effect of viscosity is neglected because the capillary network is not included in the analysis, where the viscosity has a significant effect (31). Eq. A1 can be written as

$$\begin{aligned} R_c &= K_s\left(\frac{L_s}{\left(D_s^2\right)^2} + \sum_{i=1}^{N_{\text{total}}} \frac{N_i L_i}{\left(N_i D_i^2\right)^2}\right) \\ &= K_s\left(\frac{L_s}{\left(D_s^2\right)^2} + \sum_{i=1}^{N_{\text{total}}} \frac{N_i L_i}{\left(D_s^2\right)^2 \times \left(\frac{N_i D_i^2}{D_s^2}\right)^2}\right). \end{aligned} \tag{A2}$$

To complete the derivation, we introduce the following three definitions:

1. Branching Ratio: The branching ratios ($\text{BR} = N_i/N_{i-1}$, $i = 1, \cdots, N_{\text{total}}$) are relatively constant in each level from the stem (level 0) to the smallest arterioles or venules (level N_{total}) within an organ of a given species (16,18–29), such that $N_i = \text{BR}^i$.
2. Diameter Ratio: The diameter ratio is defined as $\text{DR} = D_i/D_{i-1}$, $i = 1, \cdots, N_{\text{total}}$. It can be shown that $N_i \pi D_i^{2+\varepsilon} = N_{i-1}\pi D_{i-1}^{2+\varepsilon}$, where $\varepsilon = 0$ represents $N_i \pi D_i^2 = N_{i-1}\pi D_{i-1}^2$ area preservation from one level to the next. Conversely, $\varepsilon = 1$ represents Murray's law; i.e., $N_i \pi D_i^3 = N_{i-1}\pi D_{i-1}^3$. This provides the relation $\left(\frac{D_i}{D_{i-1}}\right) = \left(\frac{N_i}{N_{i-1}}\right)^{-\frac{1}{2+\varepsilon}}$. Therefore, the diameter ratio relates to the branching ratio as $\text{DR} = \text{BR}^{-\frac{1}{2+\varepsilon}}$ or $D_i = \text{BR}^{-\frac{i}{2+\varepsilon}} D_s$.
3. Length Ratio: The length ratio is defined as $\text{LR} = L_i/L_{i-1}$, $i = 1, \cdots, N_{\text{total}}$. West et al. (6) proposed that the perfused volume from one level to the next is approximately unchanged, so that $\frac{4}{3}\pi\left(\frac{L_i}{2}\right)^3 N_i = \frac{4}{3}\pi\left(\frac{L_{i-1}}{2}\right)^3 N_{i-1}$, which leads to the relation $\left(\frac{L_i}{L_{i-1}}\right) = \left(\frac{N_i}{N_{i-1}}\right)^{-\frac{1}{3}}$. Therefore, the relation between length ratio and branching ratio can be expressed as $\text{LR} = \text{BR}^{-\frac{1}{3}}$ or $L_i = \text{BR}^{-\frac{i}{3}} L_s$.

From Equations $N_i = \text{BR}^i$, $D_i = \text{BR}^{-\frac{i}{2+\varepsilon}} D_s$, $L_i = \text{BR}^{-\frac{i}{3}} L_s$, and Eq. A2, we obtain the following:

$$\begin{aligned} R_c &= \frac{K_s}{\left(D_s^2\right)^2}\left(L_s + L_s \times \sum_{i=1}^{N_{\text{total}}} \frac{\text{BR}^i \times \text{BR}^{-\frac{i}{3}}}{\left(\text{BR}^i \times \text{BR}^{\frac{-2i}{2+\varepsilon}}\right)^2}\right) \\ &= \frac{K_s \times L_s}{\left(D_s^2\right)^2}\left(1 + \sum_{i=1}^{N_{\text{total}}} \frac{\text{BR}^{\frac{2i}{3}}}{\text{BR}^{\frac{2i\varepsilon}{2+\varepsilon}}}\right) \\ &= \frac{K_s \times L_s}{\left(D_s^2\right)^2}\left(1 + \sum_{i=1}^{N_{\text{total}}} \text{BR}^{\left(\frac{2}{3} - \frac{2\varepsilon}{2+\varepsilon}\right)i}\right) \end{aligned}. \tag{A3}$$

Eq. A3 relates the crown resistance to the branching ratio of the vascular tree. From Taylor expansion, it is known that $\frac{1}{1-x} = 1 + x + x^2 + x^3 + x^4 + \ldots$ for $-1 < x < 1$. When $0 \le \varepsilon < 1$, the last term $\left(1 + \sum_{i=1}^{N_{\text{total}}} \text{BR}^{\left(\frac{2}{3} - \frac{2\varepsilon}{2+\varepsilon}\right)i}\right)$ can be written as $\text{BR}^{\left(\frac{2}{3} - \frac{2\varepsilon}{2+\varepsilon}\right)N_{\text{total}}} \times \left(1 + \sum_{i=1}^{N_{\text{total}}} \left(\frac{1}{\text{BR}^{\left(\frac{2}{3} - \frac{2\varepsilon}{2+\varepsilon}\right)}}\right)^i\right)$ with $-1 < \left(\frac{1}{\text{BR}^{\left(\frac{2}{3} - \frac{2\varepsilon}{2+\varepsilon}\right)}}\right) < 1$. With Taylor expansion, Eq. A3 can be written as

$$R_c = \frac{K_s \times L_s}{\left(D_s^2\right)^2} \times \mathrm{BR}^{\left(\frac{2}{3}-\frac{2\varepsilon}{2+\varepsilon}\right)N_{\text{total}}} \times \left(1 + \sum_{i=1}^{N_{\text{total}}} \left(\frac{1}{\mathrm{BR}^{\left(\frac{2}{3}-\frac{2\varepsilon}{2+\varepsilon}\right)}}\right)^i\right)$$
$$= \frac{K_s \times L_s}{\left(D_s^2\right)^2} \times \mathrm{BR}^{\left(\frac{2}{3}-\frac{2\varepsilon}{2+\varepsilon}\right)N_{\text{total}}} \times \frac{1}{1-\frac{1}{\mathrm{BR}^{\left(\frac{2}{3}-\frac{2\varepsilon}{2+\varepsilon}\right)}}}.$$
$$= \frac{K_s \times L_s}{\left(D_s^2\right)^2} \times \mathrm{BR}^{\frac{2}{3}N_{\text{total}}} \times \mathrm{BR}^{\left(-\frac{2\varepsilon}{2+\varepsilon}\right)N_{\text{total}}} \times \frac{1}{1-\left(\frac{1}{\mathrm{BR}^{\left(\frac{2}{3}-\frac{2\varepsilon}{2+\varepsilon}\right)}}\right)} \tag{A4}$$

The crown length is defined as the sum of the lengths of each vessel in the crown, such that $L_c = L_s + \sum_{i=1}^{N_{\text{total}}} N_i L_i$. Based on a similar Taylor expansion of Eq. A4, the crown length can be written as

$$L_c = L_s \times \left(1 + \sum_{i=1}^{N_{\text{total}}} \left(\mathrm{BR}^{\frac{2}{3}}\right)^i\right)$$
$$= L_s \times \mathrm{BR}^{\frac{2}{3}N_{\text{total}}} \times \frac{1}{1-\frac{1}{\mathrm{BR}^{\frac{2}{3}}}}. \tag{A5}$$

From Eqs. A4 and A5, we obtain the following equation:

$$R_c = \frac{K_s \times L_s}{\left(D_s^2\right)^2} \times \mathrm{BR}^{\frac{2}{3}N_{\text{total}}} \times \frac{1}{1-\left(\frac{1}{\mathrm{BR}^{\frac{2}{3}}}\right)} \times \left(\mathrm{BR}^{\left(-\frac{2\varepsilon}{2+\varepsilon}\right)N_{\text{total}}} \times \frac{\left(1-\frac{1}{\mathrm{BR}^{\frac{2}{3}}}\right)}{1-\left(\frac{1}{\mathrm{BR}^{\left(\frac{2}{3}-\frac{2\varepsilon}{2+\varepsilon}\right)}}\right)}\right)$$
$$= \frac{K_s \times L_c}{D_s^4} \times \left(\mathrm{BR}^{\left(-\frac{2\varepsilon}{2+\varepsilon}\right)N_{\text{total}}} \times \frac{\mathrm{BR}^{\frac{2}{3}}-1}{\mathrm{BR}^{\frac{2}{3}}-\mathrm{BR}^{\left(\frac{2\varepsilon}{2+\varepsilon}\right)}}\right). \tag{A6}$$

When $\varepsilon = 1$, we obtain

$$R_c = \frac{K_s \times L_c}{D_s^4} \times \left(\mathrm{BR}^{-\frac{2}{3}N_{\text{total}}} \times \frac{\mathrm{BR}^{\frac{2}{3}}-1}{\mathrm{BR}^{\frac{2}{3}}} \times (N_{\text{total}} + 1)\right). \tag{A7}$$

When $\varepsilon > 1$, we find

$$R_c = \frac{K_s \times L_c}{D_s^4} \times \left(\mathrm{BR}^{-\frac{2}{3}N_{\text{total}}} \times \frac{\mathrm{BR}^{\frac{2}{3}}-1}{\mathrm{BR}^{\frac{2}{3}}-\mathrm{BR}^{\left(\frac{4}{3}-\frac{2\varepsilon}{2+\varepsilon}\right)}}\right). \tag{A8}$$

If we define $K_\varepsilon = (\mathrm{BR}^{\left(-\frac{2\varepsilon}{2+\varepsilon}\right)N_{\text{total}}} \times \frac{\mathrm{BR}^{\frac{2}{3}}-1}{\mathrm{BR}^{\frac{2}{3}}-\mathrm{BR}^{\left(\frac{2\varepsilon}{2+\varepsilon}\right)}})$, $(\mathrm{BR}^{-\frac{2}{3}N_{\text{total}}} \times \frac{\mathrm{BR}^{\frac{2}{3}}-1}{\mathrm{BR}^{\frac{2}{3}}} \times (N_{\text{total}}+1))$' $(\mathrm{BR}^{-\frac{2}{3}N_{\text{total}}} \times \frac{\mathrm{BR}^{\frac{2}{3}}-1}{\mathrm{BR}^{\frac{2}{3}}-\mathrm{BR}^{\left(\frac{4}{3}-\frac{2\varepsilon}{2+\varepsilon}\right)}})$ for $0 \le \varepsilon < 1$, $\varepsilon = 1$, and $\varepsilon > 1$, respectively, Eqs. A6–A8 can be written as

$$R_c = K_s K_\varepsilon \frac{L_c}{D_s^4}. \tag{A9}$$

Finally, we set $K_c = K_s K_\varepsilon$ such that Eq. A9 can be written as

$$R_c = K_c \frac{L_c}{D_s^4}, \tag{A10}$$

where K_c depends on the branching ratio, diameter ratio, total number of tree generations, and blood viscosity.

It should be noted that although K_ε is a constant for a given crown, it does vary over the crowns due to N_{total}. We found modest variation of K_c for most vasculatures (factor of 5) except for the pulmonary tree (factor of 10). Regardless, this is a negligible variation given that the range of variables in Fig. 2 *A* is very large (eight decades on both the *x* axis and the *y* axis). In such a broad range, the relatively small variation of K_c can be neglected, as verified by the validation here.

This study was supported in part by National Institutes of Health-National Heart, Lung, and Blood Institute Grant 2 R01 HL055554-11, HL084529 and the American Heart Association Scientist Development Grant 0830181N.

REFERENCES

1. Mandelbrot, B. B. 1977. The Fractal Geometry of Nature. Freeman, New York.
2. Niklas, K. J. 1994. Plant Allometry: The Scaling of Form and Process. University of Chicago Press, Chicago.
3. Murray, C. D. 1926. The physiological principle of minimum work applied to the angle of branching of arteries. *J. Gen. Physiol.* 9:835–841.
4. Zamir, M. 1999. On fractal properties of arterial trees. *J. Theor. Biol.* 197:517–526.
5. LaBarbera, M. 1990. Principles of design of fluid transport systems in zoology. *Science*. 249:992–1000.
6. West, G. B., J. H. Brown, and B. J. Enquist. 1997. A general model for the origin of allometric scaling laws in biology. *Science*. 276:122–126.
7. West, G. B., J. H. Brown, and B. J. Enquist. 1999. The fourth dimension of life: fractal geometry and allometric scaling of organisms. *Science*. 284:1677–1679.
8. Cohen, J. E., T. Jonsson, and S. R. Carpenter. 2003. Ecological community description using food web, species abundance, and body size. *Proc. Natl. Acad. Sci. USA*. 100:1781–1786.
9. Gilooly, J. F., J. H. Brown, G. B. West, V. M. Savage, and E. L. Charnov. 2001. Effects of size and temperature on metabolic rate. *Science*. 293:2248–2251.
10. West, G. B., J. H. Brown, and B. J. Enquist. 2001. A general model for ontogenetic growth. *Nature*. 413:628–631.
11. Kassab, G. S. 2006. Scaling laws of vascular trees: of form and function. *Am. J. Physiol. Heart Circ. Physiol.* 290:H894–H903.
12. Zhou, Y., G. S. Kassab, and S. Molloi. 1999. On the design of the coronary arterial tree: a generalization of Murray's law. *Phys. Med. Biol.* 44:2929–2945.
13. Zhou, Y., G. S. Kassab, and S. Molloi. 2002. In vivo validation of the design rules of the coronary arteries and their application in the assessment of diffuse disease. *Phys. Med. Biol.* 47:977–993.
14. Kassab, G. S., and Y. C. Fung. 1994. Topology and dimensions of pig coronary capillary network. *Am. J. Physiol. Heart Circ. Physiol.* 267:H319–H325.
15. Mittal, N., Y. Zhou, S. Ung, C. Linares, S. Molloi, et al. 2005. A computer reconstruction of the entire coronary arterial tree based on detailed morphometric data. *Ann. Biomed. Eng.* 33:1015–1026.

16. Kassab, G. S., C. A. Rider, N. J. Tang, and Y. C. Fung. 1993. Morphometry of pig coronary arterial trees. *Am. J. Physiol. Heart Circ. Physiol.* 265:H350–H365.

17. Strahler, A. N. 1952. Hypsometric (area altitude) analysis of erosional topology. *Bull. Geol. Soc. Am.* 63:1117–1142.

18. Jiang, Z. L., G. S. Kassab, and Y. C. Fung. 1994. Diameter-defined Strahler system and connectivity matrix of the pulmonary arterial tree. *J. Appl. Physiol.* 76:882–892.

19. Yen, R. T., F. Z. Zhuang, Y. C. Fung, H. H. Ho, H. Tremer, et al. 1984. Morphometry of cat's pulmonary arterial tree. *J. Biomech. Eng.* 106:131–136.

20. Yen, R. T., F. Z. Zhuang, Y. C. Fung, H. H. Ho, H. Tremer, et al. 1983. Morphometry of cat pulmonary venous tree. *J. Appl. Physiol.* 55:236–242.

21. Singhal, S. S., G. Cumming, K. Horsfield, and L. K. Harding. 1973. Morphometric study of pulmonary arterial tree and its hemodynamics. *J. Assoc. Physicians India.* 21:719–722.

22. Singhal, S. S., R. Henderson, K. Horsfield, L. K. Harding, and G. Cumming. 1973. Morphometry of the human pulmonary arterial tree. *Circ. Res.* 33:190–197.

23. Huang, W., R. T. Yen, M. McLaurine, and G. Bledsoe. 1996. Morphometry of the human pulmonary vasculature. *J. Appl. Physiol.* 81:2123–2133.

24. Horsfield, K., and W. I. Gordon. 1981. Morphometry of pulmonary veins in man. *Lung.* 159:211–218.

25. Bertuglia, S., A. Colantuoni, G. Coppini, and M. Intaglietta. 1991. Hypoxia- or hyperoxia-induced changes in arteriolar vasomotion in skeletal muscle microcirculation. *Am. J. Physiol. Heart Circ. Physiol.* 260:H362–H372.

26. Ellsworth, M. L., A. Liu, B. Dawant, A. S. Popel, and R. N. Pittman. 1987. Analysis of vascular pattern and dimensions in arteriolar networks of the retractor muscle in young hamsters. *Microvasc. Res.* 34:168–183.

27. Ley, K., A. R. Pries, and P. Gaehtgens. 1986. Topological structure of rat mesenteric microvessel networks. *Microvasc. Res.* 32:315–332.

28. Koller, A., B. Dawant, A. Liu, A. S. Popel, and P. C. Johnson. 1987. Quantitative analysis of arteriolar network architecture in cat sartorius muscle. *Am. J. Physiol. Heart Circ. Physiol.* 253:H154–H164.

29. Fenton, B. M., and B. W. Zweifach. 1981. Microcirculatory model relating geometrical variation to changes in pressure and flow rate. *Ann. Biomed. Eng.* 9:303–321.

30. Huo, Y., and G. S. Kassab. 2007. Capillary perfusion and wall shear stress are restored in the coronary circulation of hypertrophic right ventricle. *Circ. Res.* 100:273–283.

31. Pries, A. R., D. Neuhaus, and P. Gaehtgens. 1992. Blood viscosity in tube flow: dependence on diameter and hematocrit. *Am. J. Physiol. Heart Circ. Physiol.* 263:H1770–H1778.

32. Christensen, K. L., and M. J. Mulvany. 2001. Location of resistance arteries. *J. Vasc. Res.* 38:1–12.

33. Chillian, W. M. 1991. Microvascular pressures and resistances in the left ventricular subepicardium and subendocardium. *Circ. Res.* 69:561–570.

34. Kanatsuka, H., K. G. Lamping, C. L. Eastham, M. L. Marcus, and K. C. Dellsperger. 1991. Coronary microvascular resistance in hypertensive cats. *Circ. Res.* 68:726–733.

35. Tillmanns, H., M. Steinhausen, H. Leinberger, H. Thederan, and W. Kubler. 1981. Pressure measurements in the terminal vascular bed of the epimyocardium of rats and cats. *Circ. Res.* 49:1202–1211.

36. Jayaweera, A. R., K. Wei, M. Coggins, J. P. Bin, C. Goodman, et al. 1999. Role of capillaries in determining CBF reserve: new insights using myocardial contrast echocardiography. *Am. J. Physiol. Heart Circ. Physiol.* 277:H2363–H2372.

37. Folkow, B. 1990. Structural factor in primary and secondary hypertension. *Hypertension.* 16:89–101.

38. Korner, P. I., and J. A. Angus. 1997. Vascular remodeling. *Hypertension.* 29:1065–1066.

39. Mulvany, M. J. 1987. The structure of the resistance vasculature in essential hypertension. *J. Hypertens.* 5:129–136.

40. Intaglietta, M., W. R. Tompkins, and D. R. Richardson. 1970. Velocity measurement in the microvasculature of the cat omentum by on-line method. *Microvasc. Res.* 2:462–473.

41. Zweifach, B. W., and H. H. Lipowsky. 1977. Quantitative studies of microcirculatory structure and function. III. Microvascular hemodynamics of cat mesentery and rabbit omentum. *Circ. Res.* 41:380–390.

42. Hudetz, A. G., C. G. M. Weigle, F. J. Fenoy, and R. J. Roman. 1992. Use of fluorescently labeled erythrocytes and digital cross-correlation for the measurement of flow velocity in the cerebral microcirculation. *Microvasc. Res.* 43:334–341.

43. Pries, A. R., T. W. Secomb, and P. Gaehtgens. 1995. Design principles of vascular beds. *Circ. Res.* 77:1017–1023.

44. Stepp, D. W., Y. Nishikawa, and W. M. Chilian. 1999. Regulation of shear stress in the canine coronary microcirculation. *Circulation.* 100:1555–1561.

45. Parthasarathi, A. A., S. A. Japee, and R. N. Pittman. 1999. Determination of red blood cell velocity by video shuttering and image analysis. *Ann. Biomed. Eng.* 27:313–325.

46. Kassab, G. S. 2005. Functional hierarchy of coronary circulation: direct evidence of a structure-function relation. *Am. J. Physiol. Heart Circ. Physiol.* 289:H2559–H2565.

47. Habazettl, H., M. Kukucka, Y. G. Weng, W. M. Kuebler, R. Hetzer, et al. 2006. Arteriolar blood flow pulsatility in a patient before and after implantation of an axial flow pump. *Ann. Thorac. Surg.* 81:1109–1111.

48. De Mesquita, J. A., Jr., E. Bouskela, E. Wajnberg, and P. L. De Melo. 2007. Improved instrumentation for blood flow velocity measurements in the microcirculation of small animals. *Rev. Sci. Instrum.* 78:024303.

49. Sada, K., M. Shirai, and I. Ninomiya. 1985. X-ray TV system for measuring microcirculation in small pulmonary vessels. *J. Appl. Physiol.* 59:1013–1018.

50. Waisman, D., A. Abramovich, V. Brod, O. Lavon, S. Nurkin, et al. 2006. Subpleural microvascular flow velocities and shear rates in normal and septic mechanically ventilated rats. *Shock.* 26:87–94.

51. Choy, J. S., and G. S. Kassab. 2008. Scaling of myocardial mass to flow and morphometry of coronary arteries. *J. Appl. Physiol.* 104:1281–1286.

52. Clark, E. R. 1918. Studies on growth of blood vessels in the tail of the frog larvae, by observation and experiment on the living animal. *Am. J. Anat.* 23:37–88.

53. Hudlicka, O., and K. R. Tyler. 1986. Angiogenesis: The Growth of the Vascular System. Academic Press, London., 221.

54. Zweifach, B. W. 1983. The microcirculation in experimental hypertension: state-of-the-art review. *Hypertension.* 5:I10–I16.